JOURNAL OF MATERIALS SCIENCE 21 (1986) 1654–1666

A diffraction approach for the study of the mechanism of 3C to 6H transformation in SiC

V. K. KABRA, DHANANJAI PANDEY
School of Materials Science and Technology, Banaras Hindu University, Varanasi-221005, India

SHRIKANT LELE
Department of Metallurgical Engineering, Banaras Hindu University, Varanasi-221005, India

Diffraction patterns taken from cubic silicon carbide crystals partially transformed to a 6H (ABCACB, . . .) structure show the presence of characteristic diffuse streaks parallel to $\mathbf{c}^*$ suggesting that the transformation takes place by statistical insertion of stacking faults. Theory of diffraction for cubic crystals undergoing transformation to the 6H structure by non-random insertion of deformation and layer displacement faults is developed separately. It is shown that a choice between the two routes of transformation can be made by comparing the theoretically predicted diffraction effects with those experimentally observed. Using such a diffraction approach, it is concluded that the transformation takes place by a non-random insertion of layer displacement faults. It is also shown that the observed diffraction characteristics cannot be explained in terms of non-random twinning through growth faults.

1. Introduction

Since the early study of Baumann [1], several workers have investigated the $\beta \rightarrow \alpha$ or 3C to 6H transformation in SiC. Recently, Pandey [2] has reviewed these investigations. In all these studies it is not clear whether the transformation occurred in the solid state or via the vapour phase. The first conclusive evidence in favour of a solid state transformation between the 3C and 6H structures of SiC was reported by Jagodzinski [3] who studied the transformation behaviour of twinned 3C-SiC crystals above 1600° C. It was found that the transformation commences with a statistical insertion of stacking faults giving rise to continuous diffuse streaks on X-ray diffraction photographs [3, 4]. Further, the final 6H structure is invariably disordered suggesting arrest of the transformation.

During the last decade, transmission electron microscope techniques have been extensively used to study the development of microstructures and the nature of the 3C/6H interface corresponding to the intermediate states of $\beta \rightarrow \alpha$ transformation in conventionally sintered, hot-pressed and reaction-sintered SiC polycrystalline samples. These investigations have been reviewed by Jepps and Page [5]. In the early stages of the transformation the α-phase morphology is a plate, having well-defined orientation relationship with the β matrix, $\{1\,1\,1\}_\beta \parallel (0\,0\,0\,1)_\alpha$ and $[1\,1\,0]_\beta \parallel [1\,1\,\bar{2}\,0]_\alpha$. In the second stage of transformation, especially in fine-grained specimens, lengthening of α-plates occurs through a coupling with grain-boundary migration involving local recrystallization of the surrounding β-grains [6–9]. This results in the formation of α-plates sandwiched by sheaths of β-phase material. Clarke [10], who also studied the morphology of the α-phase as well as the nature of the transformation interface in reaction-sintered SiC, did not, however, observe any extension of α-plates across the β-grains.

It has been reported [7, 8, 11, 12] that the $\{1\,1\,1\}$ twin interfaces of the cubic matrix provide nuclei of 6H for the initiation of the transformation which is in conformity with the X-ray observation [13] that untwinned 3C crystals do not undergo any transformation on annealing. The transformation proceeds further by the nucleation of stacking faults and their propagation by the advancement of unit-cell-high steps of 6H perpendicular to the 3C/6H habit plane [10–16]. According to Ogbuji *et al.* [15], the growth of α-SiC nuclei takes place by repeated nucleation and propagation of Shockley partials which are known to border deformation faults (for notations on stacking faults, see Pandey [17]). The 3C to 6H transformation by such a deformation mechanism is shown below schematically.

Initial structure (3C):

A B C A B C A B C A . . .
C A B C A B . . .
B C A B C . . .
A B C A . . .

Resulting structure (6H):

A B C A C B, A B C A . . . ,

where vertical bars indicate the planes across which the crystal parts have slipped past each other through a partial slip vector of the form $(a/3)\langle 1\,0\,\bar{1}\,0\rangle$. The desired Shockley partials bordering deformation faults may either be supplied by sub-grain boundaries, as envisaged by Ogbuji *et al.* [15], or may result from

0022–2461/86 $03.00 + .12 © *1986 Chapman and Hall Ltd.*

splitting of perfect dislocations. The deformation faults may also be nucleated by thermal or mechanical stresses. Once deformation faults have nucleated at correct layer positions so as to give rise to a 6H structure, their expansion above the transformation temperature is ensured by virtue of the negative stacking fault energy.

Using tilted beam crossed lattice imaging, Jepps and Page [12] have resolved the layer-by-layer stacking sequences in a range of samples of 3C-SiC partially transformed to 6H by high-temperature annealing. They have reported observation of three-layer thick twins in partially transformed 3C-SiC samples. The fact that these twins are always three layers thick implies that they are created as part of a unit process involving the displacement of a pair of layers as envisaged in the geometry of a layer displacement fault defined below:

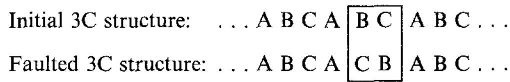

where two layers indicated by the rectangle, have transposed their orientation and thereby constitute a stacking fault. A single layer displacement fault gives rise to three layers (ACB) in twin orientation. Jepps and Page have also reported [14] little discernible strain contrast at the ends of the unit-cell-high steps of 6H in their tilted beam crossed lattice images of the incoherent 3C/6H interface. They have therefore suggested that the advancement of unit-cell-high steps at the 3C/6H incoherent interface takes place via local diffusional rearrangement of atoms in the 3C structure [5]. Any such local diffusional rearrangement of atoms in the 3C structure requires that a pair of layers be transposed since the displacement of only one layer sandwiched between two crystal halves will lead to a violation of stacking sequence principle. Geometrically it is also possible to visualize the formation of a layer displacement fault as a unit process by simultaneous nucleation and propagation of three Shockley partials on three successive planes. While the occurrence of three Shockley partials as a unit process seems to be farfetched, this process is distinct from the successive nucleation and propagation of Shockley partials envisaged in deformation mechanism. Unlike the deformation fault, which is an intrinsic fault the layer displacement fault is of extrinsic type in the sense defined by Frank [18]. This is because the faulted pair of layers do not belong to the regular structure on either side of the pair (see Pandey [17] for details). The suggestion of Jepps and Page [14] thus corresponds to 3C to 6H transformation by a layer displacement mechanism involving transposition of the orientation of a pair of layers after every four layers in accordance with the following scheme:

The present investigation was undertaken to study the mechanism of 3C to 6H transformation in SiC using a diffraction approach developed earlier by Pandey *et al.* [19–21] to elucidate the mechanism of 2H to 6H transformation in SiC. It is shown that a choice between the deformation and layer displacement mechanisms can be made from a careful analysis of the continuous intensity distribution along the streaked reciprocal lattice rows on diffraction patterns corresponding to the intermediate states of transformation. To do this we have developed the theory of diffraction from crystals undergoing 3C to 6H transformation through non-random insertions of deformation and layer displacement type of stacking faults and predicted the observable diffraction effects. From a comparison of the theoretically predicted diffraction effects with those actually observed on diffraction patterns taken from SiC crystals undergoing 3C to 6H transformation, it is shown that the transformation takes place through a non-random insertion of layer displacement faults and not by a deformation mechanism. Further, it is also shown that the observed diffraction characteristics of SiC crystals undergoing 3C to 6H transformation cannot be explained in terms of non-random twinning.

2. Principle of analysis

Following Warren [22], the general expression for diffracted intensity from a faulted cubic close-packed crystal can be written as:

$$I(h_3) = \psi^2 \sum_{m=-\infty}^{+\infty} \langle \exp(i\phi_m) \rangle \exp(2\pi i m h_3/3) \quad (1)$$

Here h_1, h_2, h_3 are continuous variables along $\boldsymbol{a}^*$, $\boldsymbol{b}^*$ and $\boldsymbol{c}^*$ reciprocal vectors corresponding to a three-layer hexagonal unit cell. ψ^2 is a function of h_1 and h_2 and vanishes except when $h_1 = H$ and $h_2 = K$, H and K being hexagonal indices with integer values. ϕ_m is the phase difference across a pair of layers, m layers apart and is given by

$$\phi_m = (2\pi/3)(H - K)q_m, \quad (2)$$

q_m being the displacement of the mth layer with respect to the origin layer in units of the stacking off-set vector which is of the type $(a/3)\langle 1\bar{1}00 \rangle$. The three possible types of pairs of layers, namely A–A, B–B, C–C; A–B, B–C, C–A and A–C, C–B, B–A, lead to three corresponding values 0, +1 and −1 for q_m. In a perfect crystal, free from stacking faults, the phase difference of the mth layer with respect to the origin layer is always fixed but for a faulted crystal it can take either of the following three values, 0, $(2\pi/3)(H–K)$ and $(-2\pi/3)(H–K)$ depending on the number, distribution and geometry of faults up to the mth layer. The average value $\langle \exp(i\phi_m) \rangle$ may be evaluated if the relative probabilities of these three phase angles can be expressed in terms of stacking fault probabilities. The evaluation of the diffracted intensity, therefore, reduces to the determination of

$$J_m = \langle \exp(i\phi_m) \rangle \quad (3)$$

for reflections with $H–K \neq 0 \pmod 3$ and is based on the statistical specification of the distribution of stacking faults. It is evident from Equation 2 that the reflections with $H–K = 0 \pmod 3$ are not affected by faulting since $\phi_m = 2\pi q_m$ and $\langle \exp(i\phi_m) \rangle = 1$. Reflections which are affected by faulting exhibit one

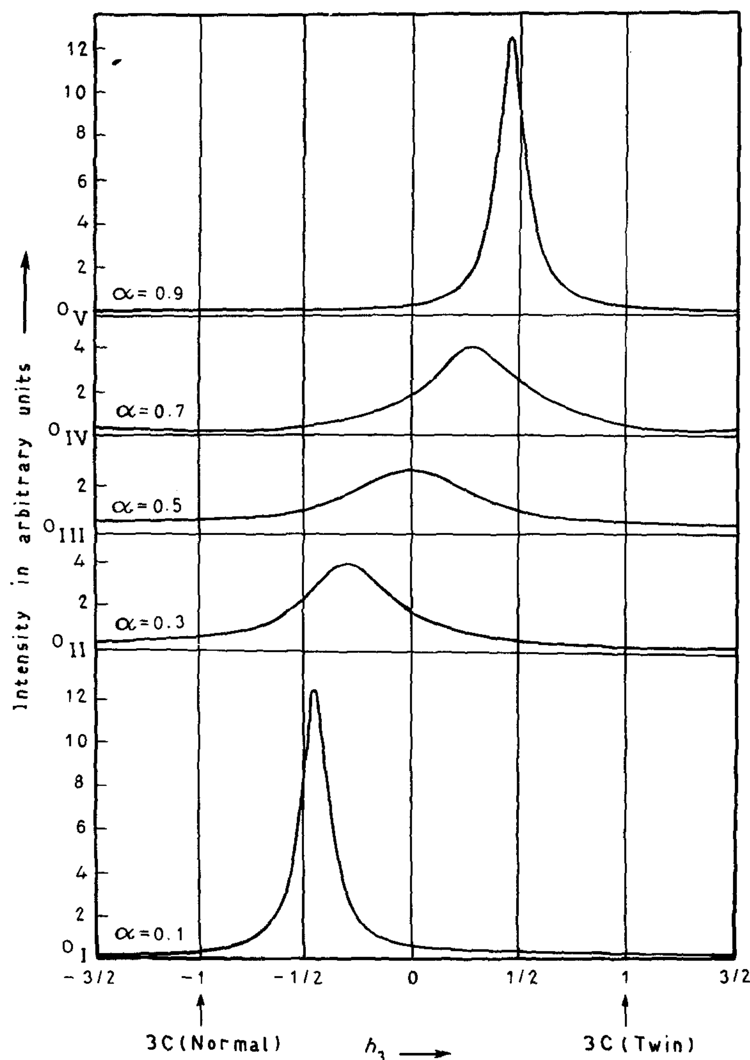

Figure 1 Variation of the calculated diffracted intensity along c^* in reciprocal space for a 3C crystal containing a random distribution of deformation faults.

or more of the following effects: (i) change in the integrated intensity; (ii) shift in peak positions; (iii) broadening of reflections; and (iv) peak asymmetry. From a measurement of these observable diffraction effects, it is possible to evaluate the type and degree of faulting which is generally characteristic of the mechanism of transformation.

3. Diffracted intensity for the deformation mechanism

Paterson [23] has developed the theory of diffraction from 3C crystals containing a random distribution of deformation faults. The intensity distribution along c^* at various h_3 values for such a randomly faulted 3C crystal is shown in Fig. 1. It is evident from the figure that as the fault probability approaches unity no new structure is formed; instead a twin configuration is generated. For the 3C to 6H transformation to take place by the insertion of deformation faults it is essential to impose a restriction on the distribution of faults. This is because when deformation faults bring about the transformation in accordance with the scheme depicted in Section 1, their distribution no longer remains entirely random. We shall take into consideration such a non-random distribution of deformation faults in developing the theory of diffraction from crystals undergoing the 3C to 6H transformation by the deformation mechanism. To do this we shall first obtain the so-called characteristic equation and the boundary conditions using the approach developed by Prasad and Lele [24] under the usual assumptions [19–21].

In a perfect 3C structure (ABC, . . .) each layer is shifted from its preceding one through a stacking offset vector of the type $(a/3)\langle 1\,0\,\bar{1}\,0\rangle$. We shall designate all such layers with subscript 0. When deformation faults are inserted in the course of the 3C to 6H transformation, five more types of layers need to be distinguished. In the schematic representation shown in Section 1, the first deformation fault has occurred after fourth layer. Introduction of a single deformation fault in a 3C crystal leads to the formation of an *hh*-contact which is known [25] to be an unstable configuration at the 3C to 6H transformation temperature in SiC and therefore must be followed by another deformation fault after the fifth layer. Accordingly the fifth layer is distinct from the 0-type layer and is assigned the subscript 1. After the fifth layer a fault may or may not occur. If a pair of faults is followed by another fault, the 3C to 6H transformation requires the absence of faults on the next three layers, i.e. they have to remain in their original orientations. So we designate the sixth, seventh, eighth and ninth layers by subscripts 2, 3, 4 and 5, respectively. The layer following the sixth layer of type 2 without the occurrence of a fault also has subscript 4. This is because its environment can be seen to be identical with that of the eighth layer. Assuming α to be the probability of

occurrence of a deformation fault involved in the 3C to 6H transformation, we can now construct the probability trees given below for transitions from $(m - 1)$th to mth layers for each of the six types of layers discussed above:

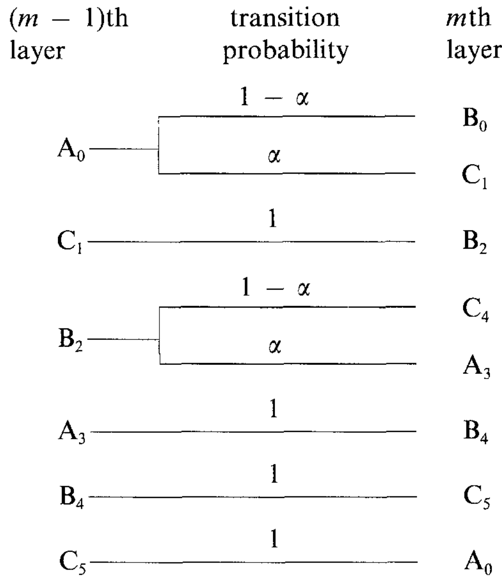

Using the above probability trees, one obtains the following characteristic equation and boundary conditions (see Appendix 1 for mathematical details):

$$\varrho^6 - \omega(1 - \alpha)\varrho^5 - \omega\alpha(1 - \alpha)\varrho - \alpha^2 = 0 \quad (4)$$

$$\begin{aligned} J_0 &= 1 \\ J_1 &= (-2\alpha + \alpha^2\omega^2 + \omega)/[(1 + \alpha)^2 + 2\alpha] \\ J_2 &= (\alpha + \omega^2 + \alpha^2\omega)/[(1 + \alpha)^2 + 2\alpha] \\ J_3 &= (1 - \alpha)^2/[(1 + \alpha)^2 + 2\alpha] \quad (5) \\ J_4 &= [(1 - \alpha)(\omega - 2\alpha\omega + \alpha)]/[(1 + \alpha)^2 + 2\alpha] \\ J_5 &= \{(1 - \alpha)[\omega^2(1 - 3\alpha) + 2\alpha(\omega - \alpha)] \\ &\quad - \alpha^2(1 + 2\alpha)\}/[(1 + \alpha)^2 + 2\alpha] \end{aligned}$$

The diffracted intensity from 3C crystals undergoing transformation to the 6H structure by deformation mechanism can now be expressed in terms of the fault probability (α) by substituting the coefficients (a) of the characteristic equation and the boundary conditions given by Equations 4 and 5, in the following expression (see Appendix 2 for mathematical details):

$$I(h_3) = \psi^2 \left[\left\{ \frac{1}{2} + \frac{\sum_{r=1}^{5} \sum_{s=0}^{r-1} a_{6-s} J_{r-s} \exp[2\pi i(6 - r)h_3/3] - a_0}{\sum_{r=0}^{6} a_r \exp[2\pi i r h_3/3]} \right\} + \{\text{complex conjugate}\} \right] \quad (6)$$

Using Equation 6, we have calculated the variation in diffracted intensity along c^* for various deformation fault probabilities (α). Since we are using a three-layer hexagonal unit cell of the 3C structure in our calculations, the 10.1, 10.2, 10.3, 10.4 and 10.5 reflections of 6H will index as $10.\frac{1}{2}$, 10.1, $10.\frac{3}{2}$, 10.2 and $10.\frac{5}{2}$ with respect to the smaller cell as depicted in Fig. 2.

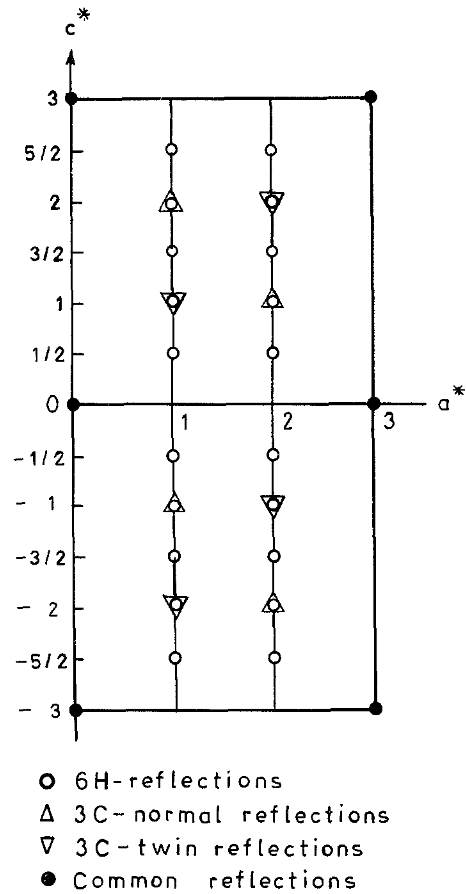

Figure 2 Reciprocal space representation of the a^*–c^* section of diffraction patterns for 3C (normal and twin) and 6H structures. The indices for 3C and 6H both are defined with respect to a three-layer hexagonal unit cell of the 3C structure.

The following diffraction effects become evident on a careful examination of Fig. 3 which depicts the calculated intensity distributions. The transformation commences with the appearance of a continuous diffuse streak joining the main 3C reflections. Right from the start, there is considerable asymmetric broadening of the 3C reflection which also exhibits some peak shift. As the transformation proceeds further, the asymmetric tail on one side of this cubic reflection gives rise to a broad-diffuse reflection which gradually approaches the normal $L = \frac{3}{2}$(mod 3) position of the 6H structure with continuously increasing peak intensity and decreasing broadening. At the same time, new peaks start emerging from the streak near $L = \frac{1}{2}$(mod 3) and 1 (mod 3) positions, which are characteristic of 6H structure. The former peak shows negative shift with small non-monotonic variation in position whereas latter one shows positive shift with monotonic variation. On further transformation, the 3C reflection becomes asymmetric on the other side of the peak and from the tail of which another reflection corresponding to $L = \frac{5}{2}$(mod 3) of 6H emerges. During the entire course of transformation, there are marked changes in the peak intensity as well as in the peak position of the

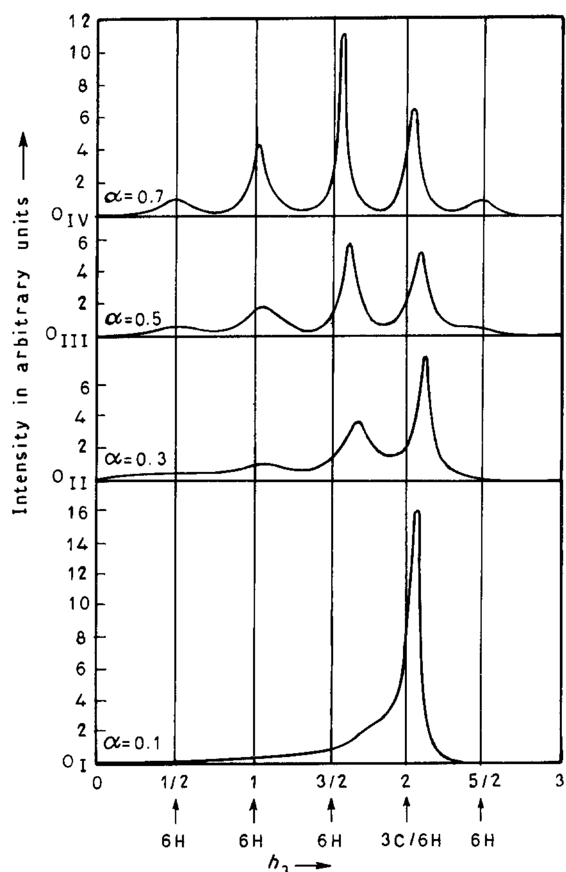

Figure 3 Variation of the calculated diffracted intensity along c^* in reciprocal space for a 3C crystal undergoing transformation to a 6H structure through a non-random insertion of deformation faults.

cubic reflection both of which fail to show a monotonic variation.

4. Diffracted intensity for layer displacement mechanism

Sato [26] has considered the theory of diffraction from a 3C crystal containing random distribution of layer displacement faults. The calculated intensity distributions along c^* for various layer displacement fault probabilities (β) are depicted in Fig. 4. The dashed vertical line represents a δ-peak whose integrated intensity varies as $(1 - \beta)/(1 + 2\beta)^2$. The continuous curve along h_3 represents the diffuse streak due to faulting. It is evident from the figure that the randomly distributed faults can generate only the twin of the starting structure, as the fault probability approaches unity. For 3C to 6H transformation to take place by the insertion of layer displacement faults, it is essential to take into account the non-random distribution of such faults, as illustrated schematically in Section 1.

As explained in the previous section, all layers in a perfect 3C structure may be assigned a subscript 0. When the layer displacement faults occur non-randomly in the course of the 3C to 6H transformation, five more types of layer should be distinguished. In the scheme showing 3C to 6H transformation in Section 1, a layer displacement fault has occurred after the fourth layer. If β is the probability of occurrence of a layer displacement fault in the 3C structure, the probability of arriving at the fifth layer with a fault will be β. Since both fifth and sixth layers have undergone displacement simultaneously to avoid any violation of the stacking rule, the probability of arriving at the sixth layer from the faulted fifth layer will be 1. The fifth layer is thus of different type as compared to layers with subscript 0. We shall assign a subscript 1 to all such layers. Once the fifth and sixth layers have undergone transposition, no layer displacement fault can occur after sixth, seventh, eighth and ninth layers if the 3C to 6H transformation has to take place. In this respect, these layers are different not only from 0 type layers but also from 1-type layers. We shall assign subscripts 2, 3, 4 and 5 to such layers.

The following probability trees can now be

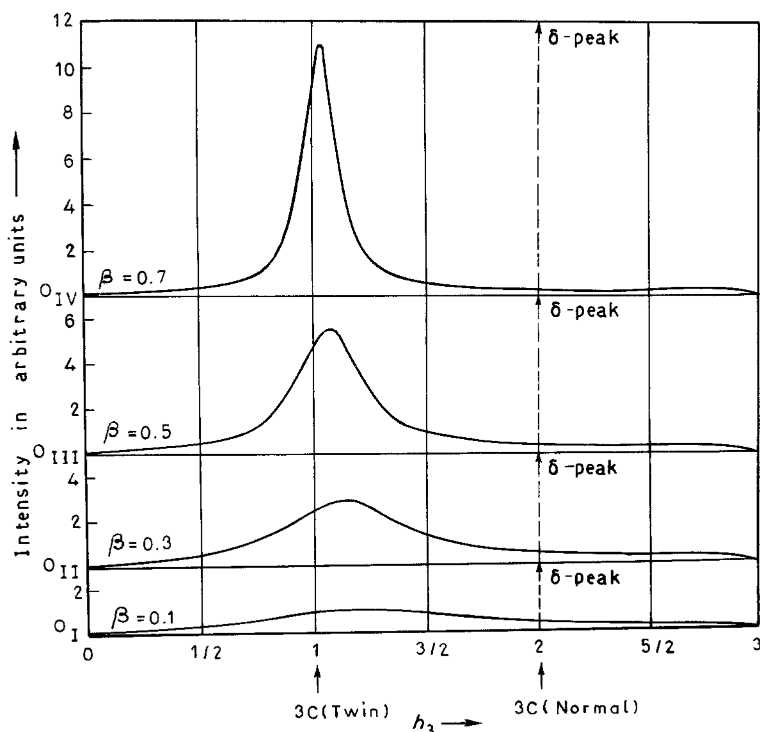

Figure 4 Variation of the calculated diffracted intensity along c^* in reciprocal space for a 3C crystal containing a random distribution of layer displacement faults.

constructed:

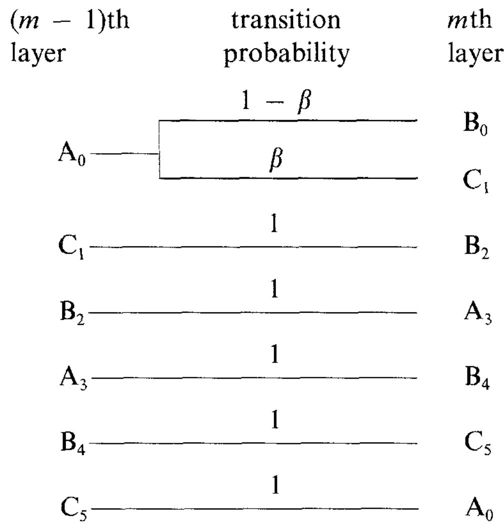

With the help of these trees and following the mathematical approach outlined in Appendix 1 for deformation faults, one can derive expressions for the characteristic equation and boundary conditions for the present case. These are given below:

$$\varrho^6 - (1 - \beta)\omega\varrho^5 - \beta = 0 \qquad (7)$$

$$\begin{aligned} J_0 &= 1 \\ J_1 &= [\omega(1 - \beta) - 3\beta]/(1 + 5\beta) \\ J_2 &= [\omega^2(1 - \beta)]/(1 + 5\beta) \\ J_3 &= (1 - \beta)/(1 + 5\beta) \\ J_4 &= [\omega(1 - \beta)]/(1 + 5\beta) \\ J_5 &= [\omega^2(1 - \beta) - 3\beta^2]/(1 + 5\beta) \end{aligned} \qquad (8)$$

Since $\varrho = \omega$ is a root of Equation 7, we shall use the following expression for the diffracted intensity in this case (see Appendix 2 for details):

$$I(h_3) = \psi^2 C_0 \sum_{m=-\infty}^{+\infty} \cos[2\pi m(h_3 + 1)/3]$$

$$+ \psi^2 \left[(1 - C_0) + \left\{ \frac{\sum_{r=1}^{4} \sum_{s=0}^{r-1} d_{5-s} K_{r-s} \exp[2\pi i h_3(5 - r)/3] - d_0 K_0}{\sum_{r=0}^{5} d_r \exp[2\pi i r h_3/3]} + \text{complex conjugate} \right\} \right] \qquad (9)$$

Here,

$$C_0 = [(1 + 2\beta)/(1 + 5\beta)]^2 \qquad (10)$$

while K and d are new sets of boundary conditions and coefficients of the characteristic equation which are free from the effect of the root wth unit modulus. These quantities can easily be derived from Equations 7 and 8 in the manner explained in Appendix 2.

Using Equation 9 we have calculated diffracted intensities for various fault probabilities (β) and the results so obtained are depicted in Fig. 5. It is evident from the figure that the transformation commences with the appearance of a continuous diffuse streak joining the main 3C reflections. The 6H peaks on the diffuse streak start developing even with a small concentration ($\beta = 0.1$) of faults but are very broad and exhibit large shifts from their normal positions. The peaks near $L = \frac{1}{2}$, 1 and $\frac{3}{2}$ (mod 3) show positive shifts whereas the peak at $L = \frac{5}{2}$ (mod 3) shows negative shift. As the concentration of faults becomes high, the peaks become more intense and less broadened and at the same time approach their regular positions i.e. positions characteristic of an ordered 6H structure. Simultaneously, the diffuse streak joining the various peaks becomes less intense. The reflection with $L = 2$ (mod 3) of the 3C structure continues to remain a δ-peak and is shown by a dashed vertical line in Fig. 5. This reflection remains sharp and unshifted throughout the transformation. However, the integrated intensity of the δ-peak, which is proportional to C_0, takes the values 0.64, 0.41, 0.33 and 0.28 for $\beta = 0.1$, 0.3, 0.5 and 0.7.

5. Comparison with experimental observations

Jagodzinski [3] has performed a detailed X-ray diffraction study of SiC crystals undergoing 3C to 6H transformation at temperatures above 1600° C. His observations have been independently confirmed by Krishna and Marshall [4]. Since the transformation is sluggish, it is possible to arrest it by simple air-quenching and study the intermediate states of transformation by X-ray diffraction at room temperature. We reproduce Fig. 6 from an article by Krishna and Pandey [13] depicting the $10.L$ reciprocal lattice row of a twinned 3C-crystal as recorded on 15° *c*-axis oscillation photographs after annealing the 3C crystal for several hours at successively higher temperatures, ranging from 1800 to 2000° C. Following observations can be made on the basis of this figure:

1. the transformation commences with a statistical insertion of faults causing the appearance of diffuse streak joining the $10.L$ reflections;
2. throughout the transformation, $10.\pm 1$ and $10.\pm 2$ reflections of 3C remain sharp although their intensities change;
3. very diffuse spots characteristic of a 6H structure start developing near $h_3 = L = \frac{1}{2}$ (mod 3) and $h_3 = L = \frac{3}{2}$ (mod 3) positions. As the transformation proceeds further, these spots sharpen and become more intense;
4. the final 6H structure is invariably disordered as revealed by the presence of diffuse streaks joining the main 3C reflections.

These observations are in agreement with those reported by Jagodzinski [3]. Fig. 7 depicts intensity distribution along the $20.L$ reciprocal lattice row of a partially transformed 3C-SiC crystal, as recorded by Jagodzinski [3]. It is evident from Figs. 6 and 7, that

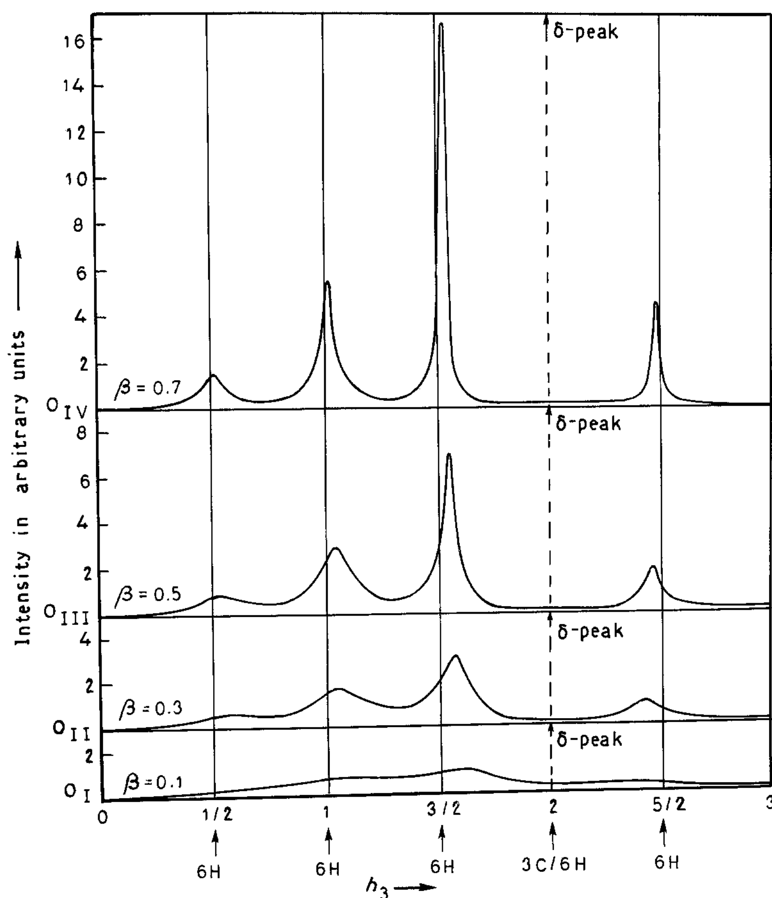

Figure 5 Variation of the calculated diffracted intensity along c^* in reciprocal space for a 3C crystal undergoing transformation to a 6H structure through a non-random insertion of layer displacement faults.

the cubic reflections remain sharp throughout the transformation and are sandwiched between diffuse reflections characteristic of the 6H structure. Jepps and Page [12] have also reported the occurrence of sharp and diffuse reflections on electron diffraction patterns recorded from partially transformed 3C crystallites. The occurrence of sharp cubic reflections sandwiched between diffuse 6H reflections has been reported by Ohta *et al.* [27] and Pandey [28] in as-grown 6H-SiC crystals obtained from vapour phase and

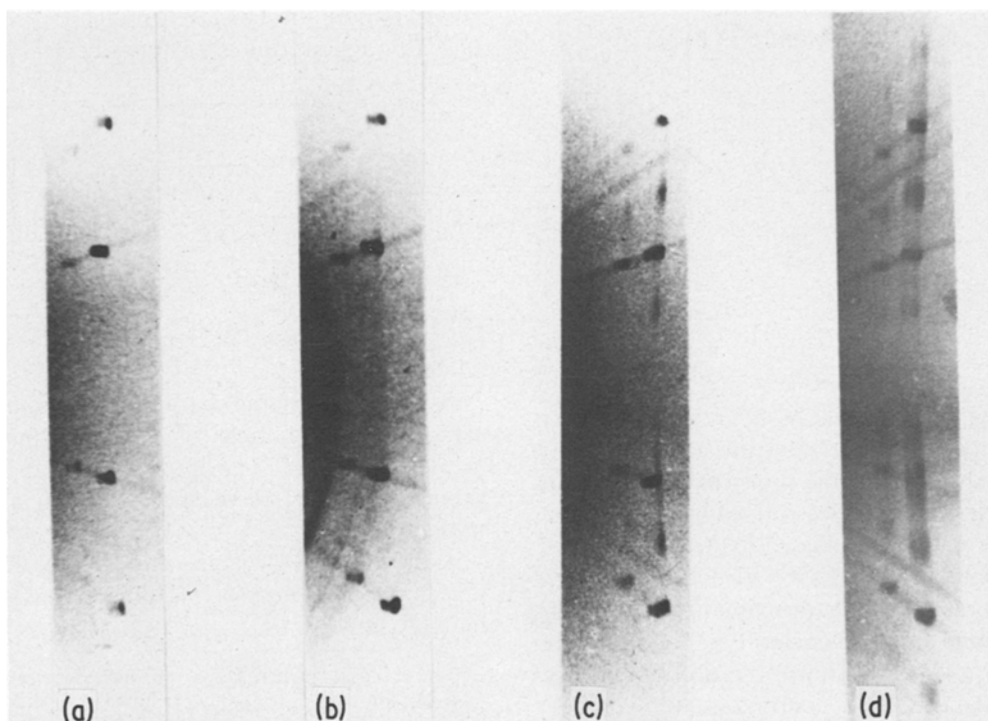

Figure 6 The 1 0 . L reciprocal lattice row of a 3C-SiC crystal as recorded on a c-axis oscillation photograph taken after successive annealing runs. Reproduced from [13]. (a) At room temperature; (b) at 1800° C after annealing for 16 h; (c) at 2000° C after annealing for another 16 h; (d) at 2000° C after annealing for another 16 h.

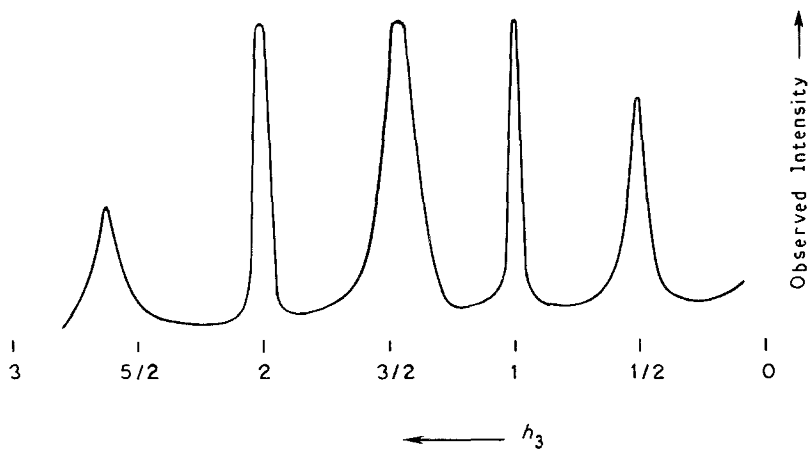

Figure 7 Linear rectified photometric trace of 2 0 . *L* reflections from a twinned 3C-SiC crystal annealed at 1800° C. After [3].

silicon melt, respectively. It is likely that these 6H crystals have resulted from 3C crystals by solid state transformation.

The facts that 1 0 . ± 1 and 1 0 . ± 2 reflections of 3C are not broadened and that diffuse elongated spots develop near $h_3 = L = \frac{1}{2}$(mod 3) and $\frac{3}{2}$(mod 3), are in agreement with the theoretical predictions of Section 4 for the layer displacement mechanism suggesting that the 3C to 6H transformation occurs by this mechanism. As pointed out in Section 3 in deformation mechanism, one would initially expect considerable asymmetric broadening of 3C reflections which with further insertion of faults will give rise to new broad reflections. Besides, the 3C reflections exhibit some shift in their peak positions. These predictions are contrary to the experimental observations of Jagodzinski [3] and Krishna and Marshall [4] described above.

6. Effect of growth faults

The calculations in Sections 3 and 4 pertain to untwinned crystals whereas the experimental observations described in the previous section are for twinned 3C-SiC crystals. A twin boundary in an as-grown 3C-SiC crystal is actually a growth fault. In the following, we shall consider the influence of a small concentration of such growth faults on the diffraction effects predicted in Sections 3 and 4. Subsequently, we shall also consider the situation where the 3C to 6H transformation is taking place by non-random insertion of growth faults only. Our calculations show that non-random twinning by growth faulting cannot explain the observed diffraction effects described in the previous section.

6.1. Small concentration of growth faults

A small concentration of growth faults implies that the normal- and twin-3C regions are quite thick. Since no streaking is observed in Fig. 6a for the twinned 3C-SiC crystal at room temperature, it is safe to assume that the thickness of individual normal-3C (ABC-type) and twin-3C (ACB-type) regions is more than 100 nm which is the coherence length for X-rays. Under such a situation, Cowley and Au [29] have shown that the diffracted intensity by a twinned crystal will be proportional to $p|F_1|^2 + q|F_2|^2$, where F_1 and F_2 are the structure amplitudes for the normal and twin counterparts, while p and q are the corresponding volume fractions for the two orientations. One can obtain the intensity distribution for the twin orientation by using the relation

$$I(H K. h_3)_{\text{normal}} = I(H K. h_3)_{\text{twin}}$$

Assuming $p = q = 1/2$, the total diffracted intensity from a twinned-3C crystal, which has been faulted subsequently, can then be obtained by adding the intensities at each point along h_3 for the normal and twin structures. Figs. 8 and 9 depict the results so

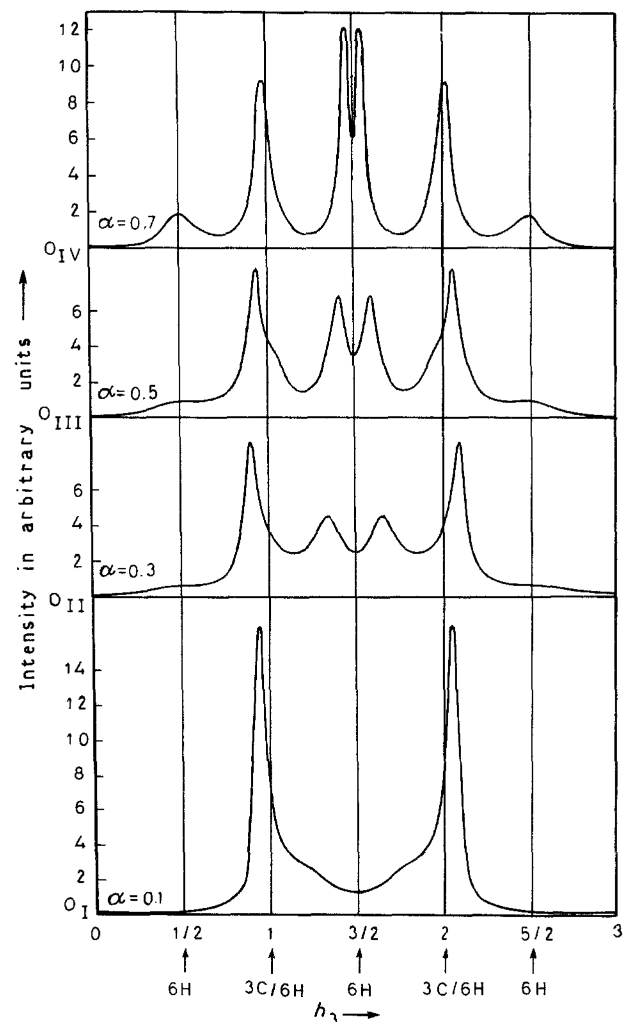

Figure 8 Variation of the calculated diffracted intensity along c^* in reciprocal space for a twinned 3C-SiC crystal undergoing transformation to a 6H structure through a non-random insertion of deformation faults.

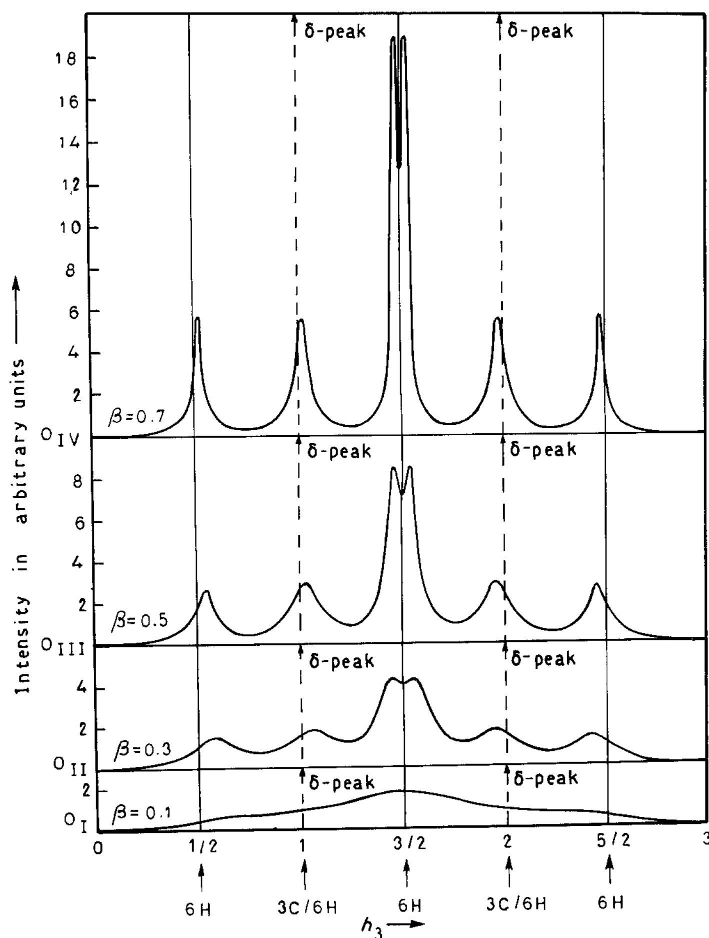

Figure 9 Variation of the calculated diffracted intensity along c^* in reciprocal space for a twinned 3C-SiC crystal undergoing transformation to a 6H structure through a non-random insertion of layer displacement faults.

obtained for a twinned 3C crystal with non-random distribution, required for the 3C to 6H transformation, of deformation and layer displacement fault, respectively.

The fact that the intensities of reflections at $L = \pm 1$ and $\pm 2 \pmod 3$ positions are almost equal in Fig. 6a, suggests that $p \approx q \approx 1/2$, and we can use the curves given in Figs. 8 and 9 for interpreting the experimental observations. It is evident from Fig. 9 that there are diffuse peaks superimposed on the infinitely sharp δ-peaks. This will, however, not lead to any qualitative as well as quantitative change in the characteristics of δ-peaks, the existence of which is sufficient to prove the involvement of layer displacement faults in twinned 3C-SiC crystals undergoing transformation to the 6H structure. It may be noted that the broad peak at $L = \frac{3}{2} \pmod 3$ in Fig. 9 exhibits two maxima surrounding a minima. It may not be usually possible to detect such a feature due to the fact that the observed X-ray diffraction patterns correspond to the convolution of the true diffracted intensity distribution with the intensity distributions due to instrumental and physical factors. Thus the presence of a small concentration of growth faults does not affect the conclusion arrived at in the previous section that the 3C to 6H transformation in SiC takes place by the layer displacement mechanism.

6.2. 3C to 6H transformation by repeated twinning through a non-random insertion of growth faults

In order to generate a 6H structure in a 3C crystal, growth faults should occur at every three layer spacings, as depicted below:

Initial 3C structure:	. . . A B C A B C A B C . . .
Intermediate structure:	. . . A B C A C B A C B . . .
Final structure (6H):	. . . A B C A C B A B C . . .

As explained in Section 3 and 4, in a perfect 3C crystal there exists only one type of layer to which we assigned a subscript 0. In the above scheme a growth fault has been introduced after the fourth layer causing all layers after the fourth layer to be in twin-orientation. Further, for a 6H structure to result, no fault should occur after the fifth and sixth layers. For this reason, we distinguish the fifth and sixth layers from the seventh layer, although all the three are in twin orientation. There is no restriction on the occurrence of a growth fault after the seventh layer. Let us assign subscripts 1, 2 and 3 to layers numbered as fifth, sixth and seventh, respectively. After the seventh layer a fault may or may not occur. The seventh layer has been labelled as 3-type because it is different from the 0-type layer in the sense that it has twin environment with respect to the succeeding layer. If a fault occurs after the seventh layer, it cannot occur after the eighth and ninth layers if the 6H structure is to be formed. The eighth and ninth layers are different from fifth and sixth layers in terms of their environment, and hence are given subscripts 4 and 5. Thus in a crystal undergoing 3C to 6H transformation by non-random insertion of growth faults, we not only have 0- and 3-type layers corresponding to the normal and twin counterparts but also 1, 2, 4 and 5-type layers. The following are the probability trees for $(m\text{-}1)$th to mth layer transitions for

this situation, with γ being the probability of non-random occurrence of a growth fault:

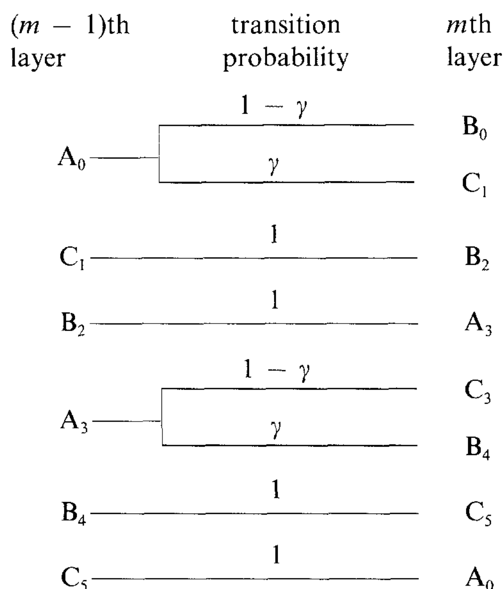

Using these probability trees, the following characteristic equation and boundary conditions have been obtained in a manner similar to that presented in Appendix 1 for deformation faults:

$$\varrho^6 + \varrho^5(1 - \gamma) + \varrho^4(1 - \gamma)^2 - \gamma^2 = 0 \quad (11)$$

$$\begin{aligned} J_0 &= 1 \\ J_1 &= -1/2 \\ J_2 &= -(1 - \gamma)/2(1 + 2\gamma) \\ J_3 &= 2(1 - \gamma)/2(1 + 2\gamma) \\ J_4 &= -(1 - \gamma)/2(1 + 2\gamma) \\ J_5 &= -(1 - 4\gamma + 6\gamma^2)/2(1 + 2\gamma) \end{aligned} \quad (12)$$

Substituting the coefficients of characteristic equation and the boundary conditions given above in Equation 6 one can calculate the intensity distribution along h_3 for various growth fault probabilities. Fig. 10 depicts the results of such a calculation. It is evident from this figure that the 3C to 6H transformation by non-random insertion of growth faults will commence with broadening of the 3C reflections at $L = \pm 1$ (mod 3) positions. This is contrary to the experimentally observed fact that the 3C reflections remain sharp throughout the course of transformation.

7. Discussion

It is evident from the foregoing analyses that the observed diffraction effects for SiC crystals undergoing 3C to 6H transformation can be explained in terms of non-random insertion of layer displacement faults only. Jagodzinski [3] has attempted to explain the occurrence of alternate sharp and diffuse diffraction maxima on X-ray diffraction patterns in terms of a model assuming a preference for twins to occur in units of three layers. However, the mathematical treatment employed by Jagodzinski does not explicitly take into account the mechanism responsible for the occurrence of twins in units of three layers. His calculations actually are aimed at simulating the desired diffraction effects without going into the mechanistic

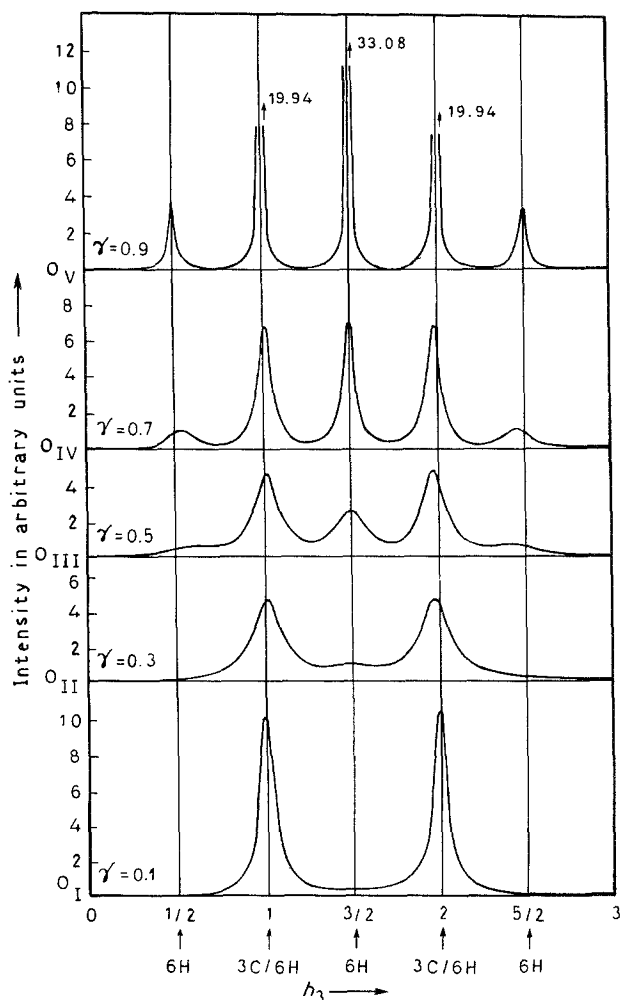

Figure 10 Variation of the calculated diffracted intensity along c^* in reciprocal space for a 3C-SiC crystal undergoing transformation to a 6H structure through a non-random insertion of growth faults.

aspect of the 3C to 6H transformation. Our approach, on the other hand, takes into account the mechanistic aspects of the 3C to 6H transformation in terms of the geometrical nature of stacking faults involved in the transformation under consideration.

As pointed out in Section 1, Ogbuji *et al.* [15] have proposed that the growth of 6H-SiC nuclei takes place by repeated nucleation and propagation of Shockley partials which are known to border deformation faults. However, our analysis shows that the deformation mechanism proposed by Ogbuji *et al.* cannot account for the observed diffraction effects unless the three Shockley partials required for the transformation recur as a unit process. The recurrence of three partials as part of a unit process seems to be a farfetched possibility and in addition is not supported by any experimental evidence. Even if one accepts this as a possibility, then following the arguments of Ogbuji *et al.* [15] no strain contrast should be visible at the 3C/6H interface since the sum of the Burgers vectors of these partials will tend to be zero in order to minimize the interfacial energy. Under such a situation the observation of Shockley partials at the transformation interfaces using ***g.b*** criterion by Ogbuji *et al.* suggests that Shockley partials are nucleated successively and not by a unit process.

The present work thus brings home a contentious point that notwithstanding the potential of TEM

technique in revealing the nature of localized defects, the features observed in isolated micrographs and the conclusions based thereupon may be misleading in as much as these do not provide a self-consistent explanation for the observed diffraction effects as well. On the other hand, except for the geometrical nature and distribution of the faults involved in the 3C to 6H transformation, it is impossible to infer anything about the nucleation of the fault or the nature of the 3C/6H incoherent interface on the basis of the diffraction approach presented in this work. In this regard, a complementary diffraction and transmission electron microscopic investigation is called for to elucidate the finer details of the mechanism of 3C to 6H transformation in SiC in a self-consistent manner.

Acknowledgement
One of the authors (D.P.) is grateful to Homi Bhabha Fellowships Council for the award of a fellowship.

Appendix 1
Derivation of characteristic equation for the deformation mechanism
The problem of calculating diffracted intensity from a faulted close-packed crystal reduces to the evaluation of $\langle \exp(i\phi_m) \rangle$ defined in Equation 1. The function $\langle \exp(i\phi_m) \rangle$ can be expressed as [24]:

$$\langle \exp(i\phi_m) \rangle = \sum P(m) \exp(i\phi_m) \quad \text{(A1)}$$

where $P(m)$ is the probability of obtaining the phase difference ϕ_m and the summation is over the three possible values of ϕ_m, namely 0, $(2\pi/3)$ and $-(2\pi/3)$ corresponding to pairs of types A–A, B–B, C–C; A–B, B–C, C–A and A–C, B–A, C–B, respectively. The probability $P(m, j)$ of finding the mth layer with subscript j (where $j = 0, 1, 2, 3, 4, 5$) is same as the probability of finding a phase difference $(\phi_m)_j$ between the mth layer with subscript j and any other type of layer at the origin. The probabilities, $P(m, j)$, can be directly written down with the help of probability trees given in Section 3, which are given below:

$$P(m, 0) = (1 - \alpha)P(m - 1, 0) + P(m - 1, 5) \quad \text{(A2)}$$

$$P(m, 1) = \alpha P(m - 1, 0) \quad \text{(A3)}$$

$$P(m, 2) = P(m - 1, 1) \quad \text{(A4)}$$

$$P(m, 3) = \alpha P(m - 1, 2) \quad \text{(A5)}$$

$$P(m, 4) = (1 - \alpha)P(m - 1, 2) + P(m - 1, 3) \quad \text{(A6)}$$

$$P(m, 5) = P(m - 1, 4) \quad \text{(A7)}$$

Let us define a function $J(m, j)$ such that

$$J(m, j) = \langle \exp(i\phi_m)_j \rangle = \sum P(m, j) \exp(i\phi_m)_j \quad \text{(A8)}$$

$J(m, j)$ can be related to $P(m, j)$ with the help of the following relation for $\exp(i\phi_m)$:

$$\exp(i\phi_m) = \exp(i\phi_{m-1}) \exp(\pm i\phi_0) \quad \text{(A9)}$$

where $\phi_0 = 2\pi/3$ is the phase difference between the $(m - 1)$th and mth layers and takes the (+) or (−) sign according as these layers are in A–B, B–C, C–A or A–C, C–B, B–A configurations. Multiplying Equation (A2) by $\exp(i\phi_m)$ and using Equations A8 and A9, we obtain:

$$J(m, 0) = (1 - \alpha) \sum P(m - 1, 0) \exp(i\phi_{m-1})_0 \times \exp(i\phi_0) + \sum P(m - 1, 5) \times \exp(i\phi_{m-1})_5 \exp(i\phi_0)$$

Writing $\exp(i\phi_0) = \omega$ and $\exp(-i\phi_0) = \omega^2$, the above equation reduces to:

$$J(m, 0) = (1 - \alpha)\omega J(m - 1, 0) + \omega J(m - 1, 5) \quad \text{(A10)}$$

In a similar way, one can obtain $J(m, j)$ for other values of j from Equations (A3) to (A7). These are given below:

$$J(m, 1) = \alpha\omega^2 J(m - 1, 0) \quad \text{(A11)}$$

$$J(m, 2) = \omega^2 J(m - 1, 1) \quad \text{(A12)}$$

$$J(m, 3) = \alpha\omega^2 J(m - 1, 2) \quad \text{(A13)}$$

$$J(m, 4) = \omega J(m - 1, 3) + (1 - \alpha)\omega J(m - 1, 2) \quad \text{(A14)}$$

$$J(m, 5) = \omega J(m - 1, 4) \quad \text{(A15)}$$

On trying a solution of the following form for the system of difference Equation (A10) to (A15):

$$J(m, j) = C_j \varrho^m, \quad m \geqslant 0, \quad \text{(A16)}$$

where C_j and ϱ are functions of α, one gets the desired characteristic equation:

$$\varrho^6 - \omega(1 - \alpha)\varrho^5 - \alpha(1 - \alpha)\omega\varrho - \alpha^2 = 0 \quad \text{(A17)}$$

Evaluation of boundary conditions
Boundary conditions are evaluated in two steps: one first obtains the probability, w_j, of finding a layer with subscript j on passing through an arbitrary region of the crystal. Then considering all possible sequences starting with layers of each type, i.e., 0, 1, 2, 3, 4 and 5 at the origin, one gets $\langle \exp(i\phi_m)_j \rangle$. From these two quantities the desired boundary conditions can easily be obtained since

$$J(m) = \langle \exp(i\phi_m) \rangle = \sum w_j \langle \exp(i\phi_m)_j \rangle \quad \text{(A18)}$$

The following relations among w can be written with the help of the probability trees, shown in Section 3 for deformation faults:

$$w_0 = (1 - \alpha)w_0 + w_5 \quad \text{(A19)}$$

$$w_1 = w_2 = w_4 = w_5 = \alpha w_0 \quad \text{(A20)}$$

$$w_3 = \alpha w_2 \quad \text{(A21)}$$

$$w_0 + w_1 + w_2 + w_3 + w_4 + w_5 = 1 \quad \text{(A22)}$$

Solving the above equations one gets

$$w_0 = \frac{1}{(1 + \alpha)^2 + 2\alpha} \quad \text{(A23)}$$

$$w_1 = w_2 = w_4 = w_5 = \frac{\alpha}{(1 + \alpha)^2 + 2\alpha} \quad \text{(A24)}$$

$$w_3 = \frac{\alpha^2}{(1+\alpha)^2 + 2\alpha} \quad \text{(A25)}$$

Using the above three equations in Equation (A18) we get the desired boundary conditions, given by Equation 5 in the main text.

Appendix 2
General expression for diffracted intensity from a faulted crystal

Let us consider a characteristic equation of the following form:

$$a_n\varrho^n + a_{n-1}\varrho^{n-1} + \cdots + a_0 = 0 \quad \text{(A26)}$$

If $\varrho_j (j = 1 \text{ to } n)$ are the roots of this equation, then following Equation A16 we have

$$J_m = \langle \exp(i\phi_m) \rangle = \sum_{j=1}^{n} C_j\varrho_j^m \quad m \geqslant 0 \quad \text{(A27)}$$

Substituting from Equation A27 into Equation 1 and after performing the summations over m, we obtain

$$I(h_3) = \sum_{j=1}^{n} [C_j + C_j\varrho_j/\{\exp(2\pi ih_3/3) - \varrho_j\} + C_j\varrho_j/\{\exp(-2\pi ih_3/3) - \varrho_j\}] \quad \text{(A28)}$$

As shown by Lele [30], the constant C_j can be evaluated from a knowledge of the boundary conditions, the coefficients of the characteristic equation and only the corresponding root ϱ_j:

$$C_j = [J_0\varrho_j^{n-1} + (J_0a_{n-1} + J_1)\varrho_j^{n-2} + \ldots + (J_0a_2 + J_1a_3 + \cdots + J_{n-3}a_{n-1} + J_{n-2})\varrho_j + (J_0a_1 + J_1a_2 + \cdots + J_{n-2}a_{n-1} + J_{n-1})] \times [n\varrho_j^{n-1} + (n-1)a_{n-1}\varrho_j^{n-2} + \cdots + 2a_2\varrho_j + a_1]^{-1} \quad \text{(A29)}$$

Knowing both, C_j and ϱ_j, one can thus obtain the desired expression for the diffracted intensity as a function of the fault probabilities.

However, it is not always possible to have analytic solutions of Equation A26. In such situations, by carrying out the summations in Equation A28, and replacing the elementary symmetric functions of ϱ_j by a_j and the expressions involving C_j by J_m, Gevers [31] (see also Holloway [32]) has obtained an expression for the diffracted intensity that involves only a_j and J_m and thus does not necessitate a solution of the characteristic equation and the evaluation of the constants C_j. Following Holloway [32], the diffracted intensity can thus be expressed as

$$I(h_3) = \psi^2\left[\left\{\frac{1}{2} + \frac{\sum_{r=1}^{n-1}\sum_{s=0}^{r-1} a_{n-s}J_{r-s}\exp[2\pi ih_3(n-r)/3] - a_0}{\sum_{r=0}^{n} a_r\exp[2\pi irh_3/3]}\right\} + \{\text{complex conjugate}\}\right] \quad \text{(A30)}$$

If p of the n roots have unit modulus, i.e. $|\varrho_j| = 1$, the summations over m in Equation 1 can be performed only for $(n - p)$ roots. Therefore, separating the series in Equation 1 after substitution of Equation A27, into two parts according as $|\varrho_j| < 1$ and $|\varrho_j| = 1$, we have

$$I(h_3) = \psi^2 \sum_{j=1}^{n-p}\sum_{m=-\infty}^{+\infty} C_j\varrho_j^{|m|}\exp(2\pi imh_3/3) + \psi^2\sum_{j=n-p+1}^{n}\sum_{m=-\infty}^{+\infty} C_j\exp(-2\pi i|m|X_j/3) \times \exp(2\pi imh_3/3) \quad \text{(A31)}$$

where the roots with $|\varrho_j| = 1$ have been expressed in the complex form, $\varrho_j = \exp(-2\pi iX_j/3)$, where X_j is an integer or proper fraction. C_j is usually real for roots with unit modulus. Denoting the second part of Equation A31 by $I_s(h_3)$, we obtain after simplifications:

$$I_s(h_3) = \psi^2\sum_{j=n-p+1}^{n}\sum_{m=-\infty}^{+\infty} C_j\cos(2\pi m/3)(h_3 - X_j) \quad \text{(A32)}$$

Thus each of the p roots with unit modulus gives rise to an infinitely sharp peak at $h_3 = X_j$, $j = (n - p + 1)$ to n.

Since Equation A30 is not valid for roots with unit modulus, elemenatry symmetric functions of only those roots for which $|\varrho_j| < 1$ need to be obtained. This can be done by dividing Equation A26 by p factors of the form $(\varrho - \varrho_j)$, $|\varrho_j| = 1, j = (n - p + 1)$ to n, giving

$$\varrho^{n-p} + d_{n-p-1}\varrho^{n-p-1} + \cdots + d_1\varrho + d_0 = 0 \quad \text{(A33)}$$

Thus a should be replaced by d in the analytic solution for the diffracted intenstity obtained by Gevers [31] and Holloway [32]. In a similar fashion, the J_m given by Equation A27, which correspond to a sum over all the roots, should also be replaced by K_m which have a sum over the roots with $|\varrho_j| < 1$ only. Thus

$$K_m = \sum_{j=1}^{n-p} C_j\varrho_j^{|m|} \quad \text{(A34)}$$

Utilizing Equation A27 we can rewrite Equation A34 as

$$K_m = J_m - \sum_{j=n-p+1}^{n} C_j\varrho_j^{|m|} \quad \text{(A35)}$$

Thus once again, one has a self-consistent set consisting of the characteristic Equation A33 and the boundary conditions A35 which no longer has the effects of any roots with unit modulus and thus can be used for calculating the diffracted intensity using the method of Gevers [31] and Holloway [32].

References

1. H. N. BAUMANN Jr, *J. Electrochem. Soc.* **99** (1952) 109.
2. D. PANDEY, *Proc. Ind. Nat. Sci. Acad.* **47** (1981) 78.
3. H. JAGODZINSKI, *Kristallogr.* **16** (1971) 1235.

4. P. KRISHNA and R. C. MARSHALL, *J. Cryst. Growth* **11** (1971) 147.
5. N. W. JEPPS and T. F. PAGE, *Proc. Cryst. Growth Charact.* **7** (1983) 259.
6. K. R. KINSMAN and S. SHINOZAKI, *Scripta Metall.* **12** (1978) 517.
7. A. H. HEUR, G. A. FRYBURG, L. U. OGBUJI, T. E. MITCHELL and S. SHINOZAKI, *J. Amer. Ceram. Soc.* **61** (1978) 406.
8. *Idem, ibid.* **61** (1978) 412.
9. S. SHINOZAKI, J. E. NOAKES and H. SATO, *ibid.* **61** (1978) 237.
10. D. R. CLARKE, *ibid.* **60** (1977) 539.
11. D. J. SMITH, N. W. JEPPS and T. F. PAGE, *J. Microscopy* **114** (1978) 1.
12. N. W. JEPPS and T. F. PAGE, *ibid.* **119** (1980) 177.
13. P. KRISHNA and D. PANDEY, *Ind. J. Phys.* Special issue (1980) 41.
14. N. W. JEPPS and T. F. PAGE, *J. Microscopy* **116** (1979) 159.
15. L. U. OGBUJI, T. E. MITCHELL and A. H. HEUER, *J. Amer. Ceram. Soc.* **64** (1981) 91.
16. S. SHINOZAKI and K. R. KINSMAN, 34th Annual Proceedings Electron Microsopy Society of America, edited by G. W. Bailey (Claitor, Baton Rouge, 1976) p. 652.
17. D. PANDEY, *Acta Crystallogr.* **B40** (1984) 567; Supplementary Publication No. SUP 39176, British Library Lending Division.
18. F. C. FRANK, *Phil. Mag.* **42** (1951) 809.
19. D. PANDEY, S. LELE and P. KRISHNA, *Proc. R. Soc. Lond.* **A369** (1980).
20. *Idem, ibid.* **A369** (1980) 451.
21. *Idem, ibid.* **A369** (1980) 463.
22. B. E. WARREN, "X-ray Diffraction" (Addison-Wesley, New York, 1969).
23. M. S. PATERSON, *J. Appl. Phys.* **23** (1952) 805.
24. B. PRASAD and S. LELE, *Acta Crystallogr.* **A27**(1971) 54.
25. P. KRISHNA and R. C. MARSHALL, *J. Cryst. Growth* **9** (1971) 319.
26. R. SATO, *Acta Crystallogr.* **20** (1966) 150.
27. K. OHTA, T. TOMITA and T. WANATABE, *Jpn. J. Appl. Phys.* **4** (1965) 652.
28. D. PANDEY, unpublished result (1975).
29. J. M. COWLEY and A. Y. AU, *Acta Crystallogr.* **A34** (1978) 738.
30. S. LELE, *ibid.* **A36** (1980) 584.
31. R. GEVERS, *ibid.* **7** (1954) 337.
32. H. HOLLOWAY, *J. Appl. Phys.* **40** (1969) 4313.

Received 29 October 1984
and accepted 4 July 1985